Iran Polym J (2016) 25:45–57
DOI 10.1007/s13726-015-0398-0

ORIGINAL PAPER

Thermoplastic starch/cellulose nanocrystal green composites prepared in an internal mixer

N. Tabassi[1] · M. R. Moghbeli[1] · I. Ghasemi[2]

Received: 5 April 2015 / Accepted: 14 November 2015 / Published online: 26 November 2015

Abstract Despite some advantages of thermoplastic starch (TPS), such as biodegradability, renewability, and low cost, it exhibits unsatisfactory mechanical properties and high vapor permeability (WVP). In this study, TPS-based green composites containing various amounts of high-stiff cellulose nanocrystals (CNCs), 0–9 wt%, were prepared in an internal mixer to modify the abovementioned drawbacks. The CNCs prepared via acid hydrolysis of microcrystalline cellulose (MCC) at different temperatures were characterized by means of scanning electron microscopy, atomic force microscopy (AFM), Fourier transform infrared spectroscopy, and X-ray diffraction analysis. The AFM micrographs showed that MCC hydrolysis at 44 °C resulted in CNCs with the highest yield of 37 % and average length and width of 272 nm and 61 nm, respectively. Adding CNC level from 0 to 9 wt% considerably increased the tensile strength of the TPS from 3.1 to 11.1 MPa (358 %), Young's modulus from 237.3 MPa to 4.2 GPa, and the glass transition temperature (T_g) from 69.2 to 90.7 °C. The relatively good interfacial interaction between CNC and TPS matrix due to rather similar polysaccharide structure in both CNC and starch caused a remarkable improvement of these mechanical properties. Furthermore, the introduction of 9 wt% CNCs decreased water vapor permeability (WVP) of the TPS from 3.4×10^{-6} to 1.3×10^{-6} g $m^{-1}h^{-1}Pa^{-1}$. In fact, the barrier effect of the CNC plates with relatively high aspect ratio decreased the WVP of the resultant nanocomposite.

Keywords Acid hydrolysis · Cellulose nanocrystals · Green composite · Internal mixer · TPS

Introduction

Starch as one of the natural thermoplastics possesses some unique properties such as biodegradability, renewability, and low cost [1]. Glycerol and water as plasticizer are mainly used to facilitate the processing of starch in general polymer processing apparatuses. Nevertheless, the prepared TPS compound usually exhibits poor mechanical and low water barrier properties [2, 3]. To improve these abovementioned drawbacks, TPS was reinforced using small amounts of stiff micro- and nanoparticles, such as silicate layers [4, 5], carbon nanotubes (CNTs) [6–8], metal oxide particles [9, 10], carbon black [11], and graphene [12, 13]. Pérez et al. [14–16] used three different kinds of layered silicates, i.e., CloisiteNa+, Cloisite30B, and Cloisite10A, to improve mechanical properties, water uptake, and creep behavior of prepared starch/polycaprolactone blends. The incorporation of Cloisite10A due to its greater compatibility with the polymer matrix led to the highest mechanical properties when compared with the other layered silicates. Mortazavi et al. [17] proposed a simple model to predict the Young's modulus of low-density polyethylene (LDPE)/TPS blends containing various amounts of Cloisite30B. Their results showed a good agreement between the model and experimental results. Liu et al. [18] prepared high-performance TPS/carboxylate multi-wall carbon nanotube (CMWNT) nanocomposites using plasticized residue cornstarch granules as a polymer matrix. The tensile results indicated that

✉ M. R. Moghbeli
mr_moghbeli@iust.ac.ir

[1] School of Chemical Engineering, Iran University of Science and Technology (IUST), Tehran 16844–13114, Iran

[2] Plastic Department, Iran Polymer and Petrochemical Institute, Tehran 14965–115, Iran

the applied load was properly transferred from the matrix to the ultra-strong functionalized carbon nanotubes. Glycerol-plasticized pea starch biocomposite films reinforced with various graphene oxide (GO) levels were prepared by Li et al. [19]. The introduction of GO in the plasticized starch increased the tensile strength and Young's modulus, while reducing moisture uptake of the resultant nanocomposite films.

Recently, CNCs and cellulose nanowhiskers have been used as proper candidates to enhance the TPS mechanical and barrier properties. These reinforced materials with complete biodegradability were classified as green composites which offer great potential to be used in food packaging or biomedical industry. CNCs are commonly produced from natural resources via mechanical treatment and acid hydrolysis [20]. The morphology and geometry of CNCs depending on hydrolysis conditions influence their performance as a reinforcement. The most important crucial hydrolysis parameters are hydrolyzing temperature [21] and time [22, 23], cellulose and acid concentrations [24, 25]. Some research works focused on using cellulose microfibers and nanofibrils [26–28], cellulose particles and crystals [29, 30] as reinforcing agents to improve the physical and mechanical properties of TPS. The addition of CNCs up to 5 wt% to glycerol-plasticized wheat starch improved the tensile strength and thermal stability, and reduced the water vapor permeability of casting nanocomposite films [31]. Kaushik et al. [32] showed that the addition of cellulose nanofillers up to 10 wt% improved water barrier property, while further addition deteriorated the property due to possible fiber agglomeration. Aila-Suárez et al. [33] reported that the incorporation of CNCs in starch films improved some mechanical, barrier, and functional properties. González et al. [34] added simultaneously the waxy starch nanocrystals (WSNCs) and cellulose nanocrystals (CNCs) to thermoplastic maize starch. The incorporation of CNC and CNC/WSNC considerably improved the mechanical properties, but no significant differences in barrier properties were observed. Prakobna et al. [35] prepared core–shell amylopectin (AP)-coated cellulose nanofibers and amylopectin/cellulose nanofiber nanocomposites to investigate the effect of AP matrix distribution on the moisture barrier and ductile properties of resulting biofilms. The core–shell nanofibers exhibited the exceptional performance when compared with the nanocomposites prepared with more irregular AP distribution.

The goal of this research is to prepare TPS/CNT biodegradable composites with proper mechanical and moisture barrier properties. Using these thermoplastic composites with improved properties could minimize the generation of pollution in various applications such as food packaging, because most synthetic thermoplastics currently are non-degradable. Although some researchers have investigated the effect of CNCs on the mechanical and barrier properties of TPS nanocomposite films prepared via casting process, less attention has been paid to the use of melt mixing process [36, 37]. In this research work, the CNCs were extracted from MCC via acid hydrolysis. The effect of hydrolysis time and temperature on the structural and morphological characteristics and conversion of the produced CNCs was investigated. Thereafter, TPS composites containing various amounts of CNCs were prepared in an internal mixer at a processing temperature above the gelatinization of the starch. The effect of CNC level on the tensile and dynamic mechanical properties and water vapor permeability of the resultant composites was investigated.

Experimental

Materials

All chemical reagents were prepared from Merck Co. (Darmstadt, Germany), unless otherwise stated. MCC and sulfuric acid (98 wt%) were used for hydrolysis. Corn starch (Alvand Conversion Industries Co., Hamedan, Iran), glycerol (Asia Exir Co., Tehran, Iran), and potassium carbonate (K_2CO_3) were purchased. Stearic acid (Aba Chemistry Co., Tehran, Iran) was used as an external lubricant. Dialysis bag membrane (12 kD, Caspian Co., Tehran, Iran) was prepared. Distilled deionized water (DDI) as a CNC dispersion medium was purchased from Zolal Teb Shimi Co. (Tehran, Iran).

CNC preparation

First, a given amount of MCC dispersed in DDI was poured into a 100-ml flat-bottom glass reactor equipped with a gas purge inlet, overhead stirrer, condenser, and feeder (Fig. 1). The reactor was placed in a bath with a thermostatic control. Thereafter, the acid was added dropwise into the suspension which was stirred at 120 rpm. The recipes of the hydrolysis dispersion are summarized in Table 1. The dispersion was then immediately heated to reach to a desired temperature of hydrolysis. The stirring was continued for a given hydrolysis time and the temperature was precisely controlled by a thermometer during the process. As it is well known, the temperature is a crucial parameter of hydrolysis process and drastically depends on the cellulosic source. Most researchers selected hydrolysis temperatures and time in the range of 40–50 °C and 10–240 min, respectively [24, 25, 38]. In this research work, the hydrolysis of MCC was carried out at various temperatures (40, 44, 48, and 52 °C) for an optimum time of 130 min, while other effective parameters were set to the values reported previously.

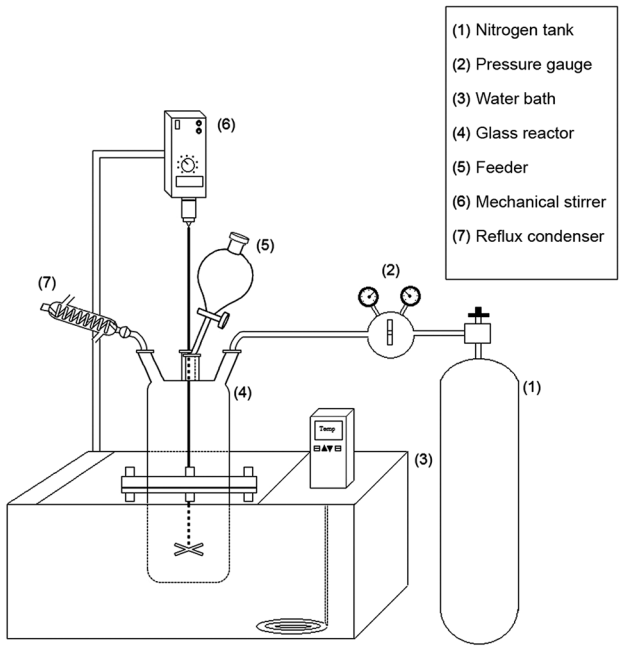

Fig. 1 Schematic representation of batch reactor setup for acid hydrolysis of MCC

Table 1 Process parameters for MCC hydrolysis

Run	Temperature (°C)	H_2SO_4 conc. (%)	Time (min)	MCC Disp. (g/100 ml)	Sonication time (min)
1	40	63.5	130	10.2	30
2	44				
3	48				
4	52				

After hydrolyzing, the reactor was immediately placed in an ice-salt cooling bath. The suspension was held without any mixing and shaking for further 24 h at room temperature to separate the suspension into sediment and supernatant phases. After sedimentation of the solid phase, the supernatant was removed from the sediment and replaced with fresh DDI portion. The DDI replacement was repeated four times to increase the pH until the supernatant phase is disappeared and a uniform dispersion is observed. This washing and stabilizing process prevents the probable aggregation of CNCs. The suspension was then centrifuged for 15 min at 9000 rpm in an ultra-centrifuge (Sigma, 2–16 K, Germany). Similar to the previous step, the supernatant was removed each time to be replaced by a new fresh DDI portion. This cycle was repeated until the supernatant became turbid. Finally, the pH of the suspension was stabilized at a constant value close to neutral range using the dialysis bag membrane. For this purpose, the deionized water was renewed every 24 h in order to keep the maximal ion exchange driving force. Thereafter, the neutralized CNCs were delaminated using an ultrasonic homogenizer (Bandelin, HD 3200, Probe KE76, Germany). The specimen vial was placed in an ice bath to restrain the excessive temperature increase during sonication. Undesirable overheating may desulfate the CNCs' sulfate groups [23]. The final homogenized suspension was dried in a freeze-dryer (Sigma, RVC 2-18 CD plus, Germany) for 24 h to form a white cotton-like solid. The yield of the process was calculated according to the weight of dried solid contents before and after hydrolysis.

Preparation of TPS/CNC nanocomposites

Corn starch and glycerol as plasticizer were used for preparation of the neat TPS and its nanocomposites with various CNC levels. The glycerol content on the base of TPS was fixed at 22 wt%. For preparing nanocomposites, various amounts of CNCs ranging from 0 to 9 wt% were added to the base ingredients. The mixing process was carried out in an internal mixer (W50 Brabender, Germany) at 115 °C and rotor speed 100 rpm for 8 min. The dried CNCs were added to the base ingredients, i.e., starch and glycerol, to prepare corresponding TPS/CNC nanocomposites. The recipes for preparation of the neat and reinforced TPS composites are listed in Table 2. After mixing, the specimens were compression molded in a hot press apparatus (Toyoseiki, Mini Test Press, Japan) at 180 °C and 35 MPa. The hot press apparatus was equipped with electrical elements for warming and water circulation system for cooling processes. The tensile test specimens were prepared under ASTM D638 protocol. DMTA test specimens with $1 \times 1.5 \times 120$ mm^3 dimensions were used to study the dynamic mechanical properties of the neat and reinforced TPS specimens. All the test specimens were stored in a desiccator with a relative humidity of 43 ± 0.5 % using the saturated potassium carbonate solution according to ASTM E104 standard protocol for 2 weeks before mechanical test.

Table 2 Recipes for TPS and its composites with various CNC levels

Code	Starch (wt%)	Glycerol (wt%)	CNC (phr)
TPS	78	22	0
TPS + 1 % CNC	78	22	1
TPS + 3 % CNC	78	22	3
TPS + 5 % CNC	78	22	5
TPS + 7 % CNC	78	22	7
TPS + 9 % CNC	78	22	9

CNC characterization

Morphology

Morphology of the CNCs was studied using scanning electron microscopy (SEM, Vega II Tescan, Czech Republic). The solid content of CNC dispersion was diluted up to 0.01 wt%, and then a droplet was put on a glass lamella at room temperature and dried for 2 h. Surface of the dried specimens was coated with a very thin layer of gold before microscopy observation since the non-conducting wood nanofibers invariably lead to uncontrollable charging effects and poor topographical resolution. The precise geometry and morphology of the produced CNCs were also studied with a DME atomic force microscope (AFM) (Dual scope 95-200E, Denmark) [39]. In this study, a droplet of diluted dispersion was poured onto the surface of a mica thin sheet which was able to absorb CNCs.

Chemical and crystalline structure

A Fourier transform infrared spectrometer (FTIR, Perkin Elmer, spectrum RX1, USA) was used at 2 cm^{-1} resolution in order to study the chemical bonds and functional groups of the CNCs prepared through acid hydrolysis process. The crystalline structure of both MCC particles and CNCs was studied by an X-ray diffractometer (XRD, Jeol, JDX-8030, Japan) using copper Kα (CuKα) radiation with a wavelength (λ) of 1.5416 Å. For this purpose, MCC and CNC dried powders were tightly pressed into a cylindrical sample holder. The analysis was performed between the angles of incidence $2\theta = 5°$ and 40°. The crystallinity (X_c) and crystallinity index (I_c) values were calculated based on the following equations as follows [28, 40]:

$$X_c = \frac{I_{(cr\,002)} - I_{(cr\,101)}}{I_{(cr\,002)}} \times 100 \quad (1)$$

$$I_c = \frac{I_{(cr\,002)} - I_{(am)}}{I_{(am)}} \times 100, \quad (2)$$

where $I_{(cr\,002)}$ is the peak intensity at $2\theta \approx 20°$, $I_{(cr\,101)}$ is the peak intensity at $2\theta \approx 16°$, and $I_{(am)}$ is the peak intensity at $2\theta \approx 18°$. $I_{(cr\,002)}$ and $I_{(cr\,101)}$ represent the (002) and (101) crystalline plates, respectively, while $I_{(am)}$ is the indicator of minimum intensity of X-ray diffractograms between the peaks (002) and (101). It is well known that $I_{(cr\,002)}$ is a representative of both crystalline and amorphous regions, while $I_{(am)}$ shows only the amorphous domains.

Mechanical properties of TPS/CNC nanocomposites

Mechanical tensile behavior of the neat and CNC-reinforced TPS specimens was determined using a universal testing machine (Jinan Tianchen model WDS-10A, China) with a cross-head speed of 1 mm/min at room temperature. Dynamic mechanical behavior of the neat TPS and its nanocomposite specimens was measured with a 2000 DMTA (Triton technology, England). The test was carried out in bending mode at the frequency of 1 Hz, a heating ramp of 4 °C min^{-1}, and the temperature ranging from −100 to +150 °C. The glass transition temperature (T_g) was determined based on the temperature of maximum loss tangent peak.

Water vapor permeability (WVP)

Water vapor permeability of the neat TPS and TPS/CNC nanocomposites was determined based on ASTM E96 standard method. For this purpose, 4-mm-diameter circle disks were cut from the films with 1 mm thickness. For WVP performance of the TPS and its composites with CNCs, a given amount of dried anhydrous calcium chloride ($CaCl_2$) was placed into a glass vial. In this case, the vial was enclosed by the disk and sealed with paraffin wax. Thereafter, all the filled vials were put in a desiccator containing saturated vapor at 30 °C. Penetration of the water vapor through the films increased the weight of the absorbent. Actually, $CaCl_2$ is a desiccant which absorbs the transferred water vapor. Weight changes of the cells were recorded as a function of time. Water vapor transmission rate (WVTR) (g h^{-1} m^{-2}) of the neat TPS and nanocomposite films was calculated using linear regression of weight–time curves using the following equation:

$$\mathrm{WVTR} = \frac{S}{A}, \quad (3)$$

where S is the slope of weight versus time curve (g/h) and A is the transfer area (m^2). WVP (g m^{-1} h^{-1} Pa^{-1}) was finally calculated according to the following equation:

$$\mathrm{WVP} = \frac{\mathrm{WVTR}}{P(R_1 - R_2)} \times D, \quad (4)$$

where P is the saturation vapor pressure of water (Pa) at 30 °C, R_1 and R_2 are the relative humidity (RH) in the desiccator and permeation vial, respectively, and D is the thickness of the disk (m). Since P is 4243 Pa in 30 °C, the driving force of water diffusion [$P(R_1-R_2)$] was 4243 Pa.

Results and discussion

CNC characteristics

Morphology

Figure 2a indicates SEM micrographs of the MCC particles. As shown in the figure, the size of microcrystals varied from 5 to 20 μm. Hydrolyzing the MCC at the temperatures of 40 and 52 °C resulted in the formation of CNCs. The CNCs have a mean length of about 500 nm when prepared at the former temperature (Fig. 2b). On the contrary, increasing the hydrolysis temperature to 52 °C broke down the MCC particles into very small nanoparticles with spherical morphology (Fig. 2c). The accelerated degradation of cellulose macromolecules at 52 °C led to nanoparticles with the lowest aspect ratio and spherical geometry. In this case, the lower aspect ratio may limit the application of CNCs as a suitable reinforcement. Additionally, AFM analysis was used to investigate clearly the effect of hydrolysis temperature on the geometry of the resultant CNCs.

Figure 3 shows the AFM images of the CNCs prepared at 40, 44, and 48 °C. The images exhibited rod-shape morphology of the nanoparticles synthesized at the hydrolysis temperatures below 52 °C. Nevertheless, increasing the hydrolysis temperature decreased the length of the CNCs. The mean length, width, aspect ratio, and yield of CNCs are summarized in Table 3. As can be seen, the average length and width of the CNCs prepared at 40 °C were 547 and 149 nm, while increasing the temperature to 48 °C decreased the average length and width to 131 and 56 nm, respectively. This reduction may be attributed to the intensive cellulose degradation at higher temperature. A mean length of 272 nm and width of 61 nm was observed for the CNCs hydrolyzed at 44 °C. At this temperature, the highest values of aspect ratio and conversion rate were obtained when compared with those at other hydrolysis temperatures.

Figure 4 indicates the size distribution of the CNCs. As shown, the increase in temperature shifted the distribution curve to lower particle sizes. The narrowest size distribution curve with the lowest mean length was observed for the CNCs prepared at higher hydrolysis temperature, i.e., 48 °C. This behavior can be due to breakdown the longer CNCs into smaller ones when the temperature increases. In addition, the yield of the hydrolysis reaction was slightly decreased with increasing the temperature from 40 to 44 °C, while the aspect ratio increased to some extent. Lower aspect ratio at lower temperature can be attributed to insufficient hydrolysis of the amorphous regions in the MCC structure [21]. In contrast, further increase in hydrolysis temperature from 40 to 52 °C considerably decreased

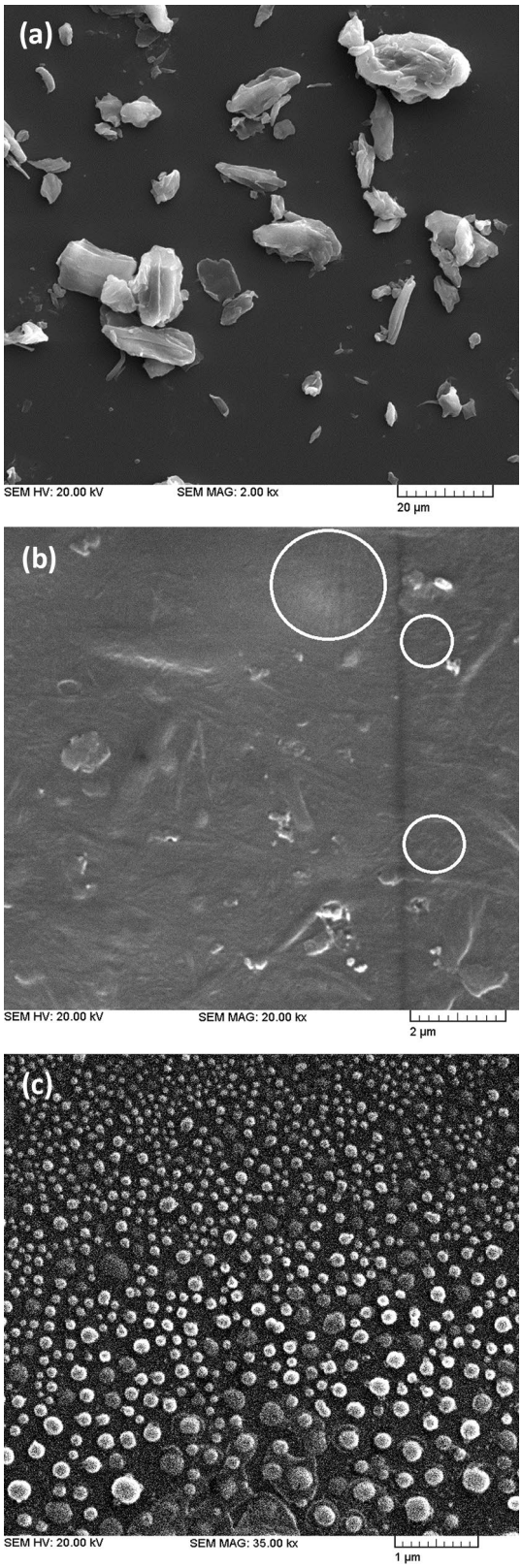

Fig. 2 SEM micrographs of **a** the MCC and its hydrolyzed products **b** at 40 °C and **c** at 52 °C

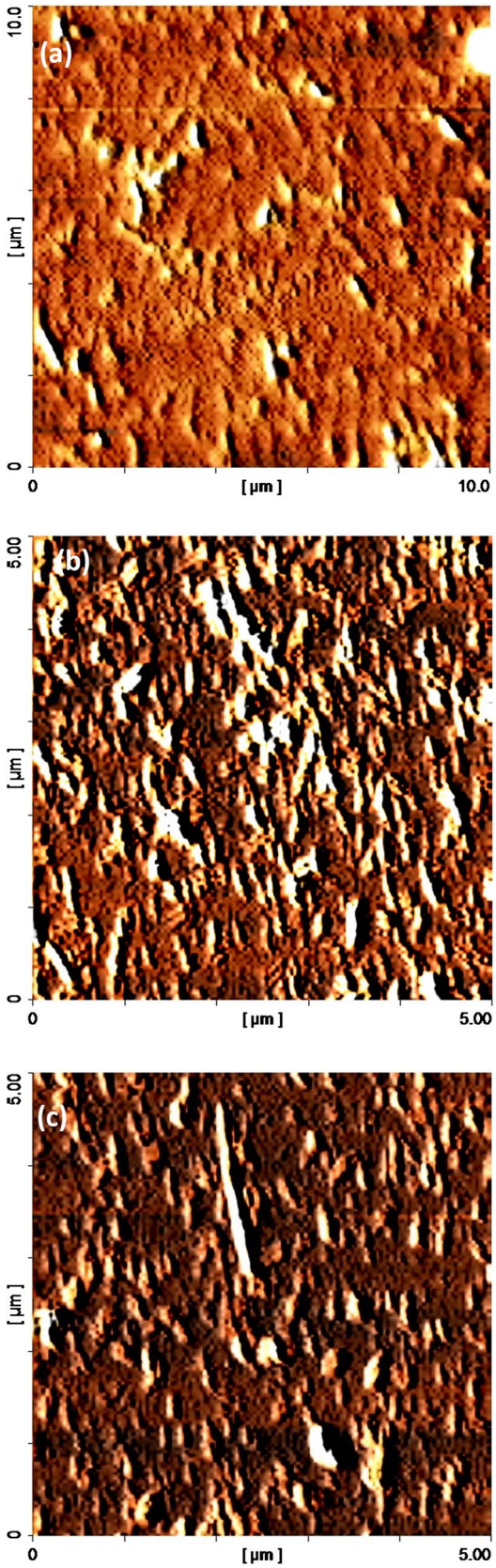

Fig. 3 AFM images of the CNCs produced at various hydrolysis temperatures: **a** 40, **b** 44, and **c** 48 °C

the conversion from 41.2 to 9.9, respectively. Indeed, the CNCs prepared at 44 °C with the highest aspect ratio and relatively high conversion were selected to reinforce the TPS.

Chemical structure

FTIR analysis was performed to identify the chemical structure of the MCC and CNCs (Fig. 5). As shown, for the MCC the absorption peaks at 1058 and 1108 cm^{-1} are attributed to the C–O bond stretching of the C–O–C and C–O–H groups, respectively. These peaks in the CNC spectra shifted to higher wave numbers of 1062 and 1124 cm^{-1}, respectively. In addition, the absorption peak of OH groups also shifted to a lower wave number, 3442 cm^{-1}, in the CNC structure. It seems that the hydrogen-bonding interaction among the cellulose molecules was weakened during the hydrolysis process and, consequently, led to a blueshift (Fig. 5). Both materials showed peaks at 1640 and 2890 cm^{-1} which correspond to the OH groups of the absorbed water and H–C–H bonds, respectively. Interestingly, there was a small peak at 1430 cm^{-1} on the MCC spectra which is just disappeared on the CNC spectra. This peak is related to methoxyl groups which are indicative of the presence of lignin in the MCC structure. It means that the lignin was removed from the CNC structure after acid hydrolysis process.

Crystalline structure

X-ray diffraction pattern was used to determine the crystalline structure of both MCC and CNCs. Figure 6 indicates the diffractograms of the neat MCC and MCC hydrolyzed at 44 °C. As seen, the MCC pattern exhibits a sharp peak at a diffraction angle of 22.4°, two overlapped sharp peaks at 14.7° and 16.1°, and a weak peak centered at 34.4°, which are attributed to crystalline planes (200), (101), (101), and (004), respectively [41]. The crystalline plane (200) observed in the MCC pattern represents the crystalline structure of the typical cellulose I. In the CNC structure, only a wider peak at $2\theta = 22.2°$ is obvious. This peak may be related to the formation of another new crystalline structure, i.e., cellulose II [42]. Disappearance of the peaks at the planes (101) and (004) is due to the fact that most of the amorphous domains are removed from the MCC, while cellulose I is maintained in the CNC structure. The crystallinity levels of the MCC and CNCs were 65.9 and 81.8 %, while their crystallinity index was 89.2 and 77.7 %, respectively. In fact, hydrolyzing the MCC seems to increase the crystallinity percentage while decreasing the crystallinity index. Since the crystallinity index corresponds to (002) crystal plane level, this difference can arise from the

Table 3 Characteristics of the CNCs prepared at different hydrolysis temperatures

Temperature (°C)	Length of CNCs (nm)	Width of CNCs (nm)	Aspect ratio	Yield (%)
40	547 ± 153	149 ± 35	3.67	41.2
44	272 ± 129	61 ± 23	4.46	37.4
48	131 ± 46	56 ± 12	2.34	18.4
52	No whisker	No whisker	–	9.9

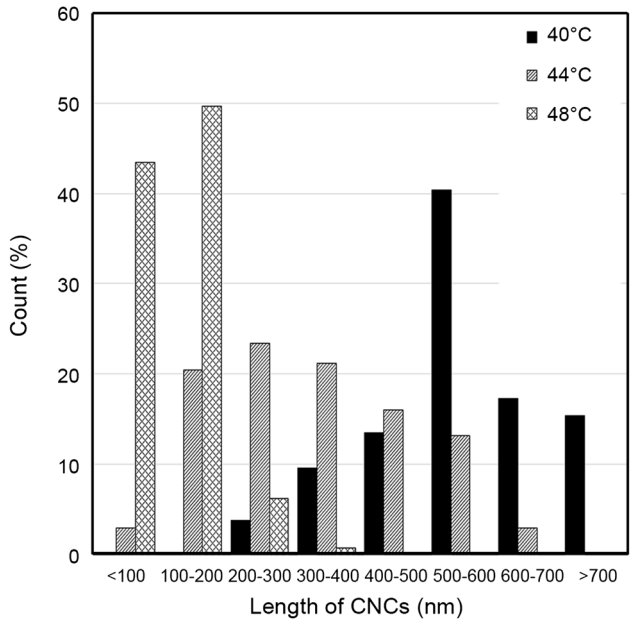

Fig. 4 Size distribution of the CNCs hydrolyzed at 40, 44, and 48 °C

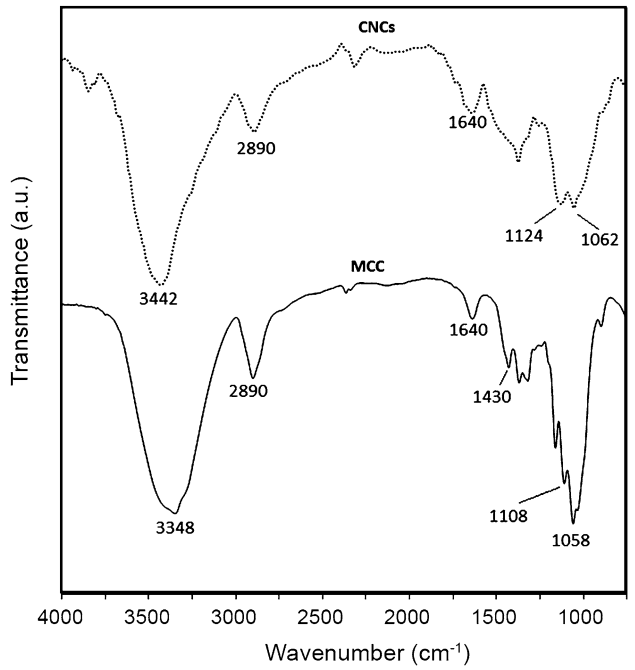

Fig. 5 FTIR spectroscopy of the MCC (*lower spectra*) and CNCs prepared at a hydrolysis temperature of 44 °C (*upper spectra*)

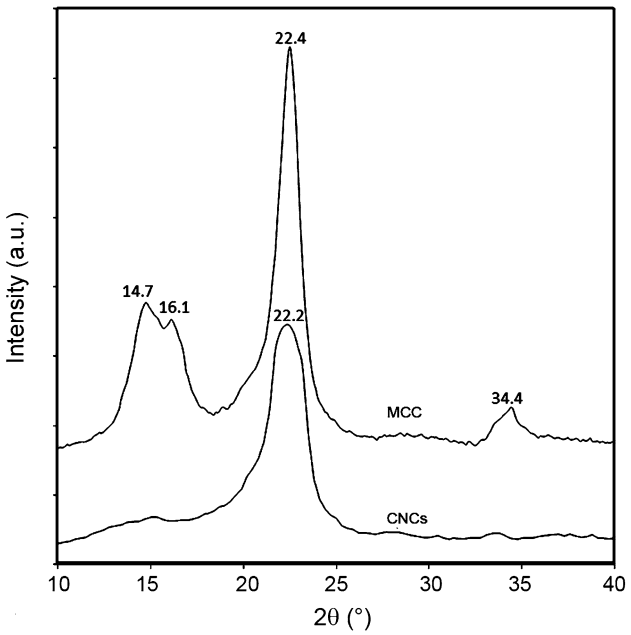

Fig. 6 XRD patterns of the MCC and CNCs prepared at a hydrolysis temperature of 44 °C

presence of the other new types of crystalline structures in the CNCs.

Effect of CNC level on applied torque

The measurement of the torque value in an integral mixture as a processing parameter could indicate the morphological stability of blends or composite systems during mixing. In fact, measuring stable torque in a plateau region reflects a balance between the rate of creation and the breakdown of aggregates in molten state, which may indicate the stabilized dispersion state. Figure 7 shows the torque variation of the neat TPS and its composites with various CNC levels during blending process. Two regions were observed on the TPS torque variation curve. Adding the semi-crystalline starch with a given amount of the plasticizer to the internal mixer increased the torque value to 70 N.m. However, diffusing the plasticizer into the granules by the elapsed time of mixing and consequently melting the crystal regions decreased the applied torque to 40 N.m where the mixing process was stopped. Different CNC levels, 1–9 wt%, were

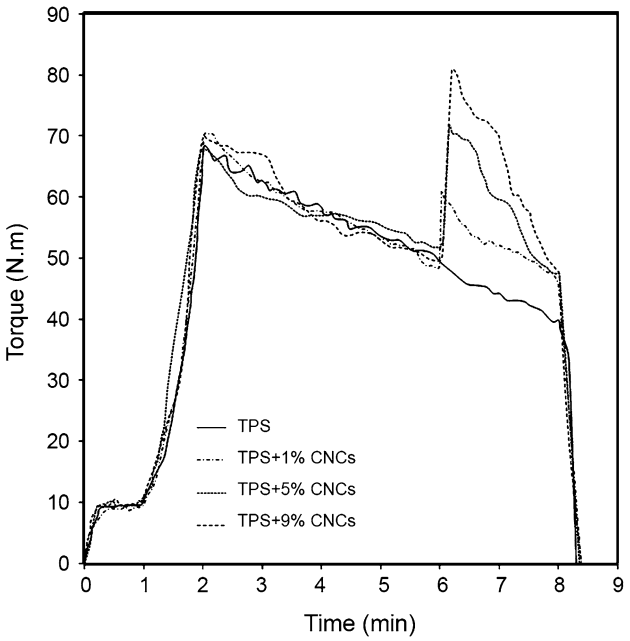

Fig. 7 Torque variation versus mixing time for the preparation of the neat TPS and TPS/CNC nanocomposites in an internal mixer

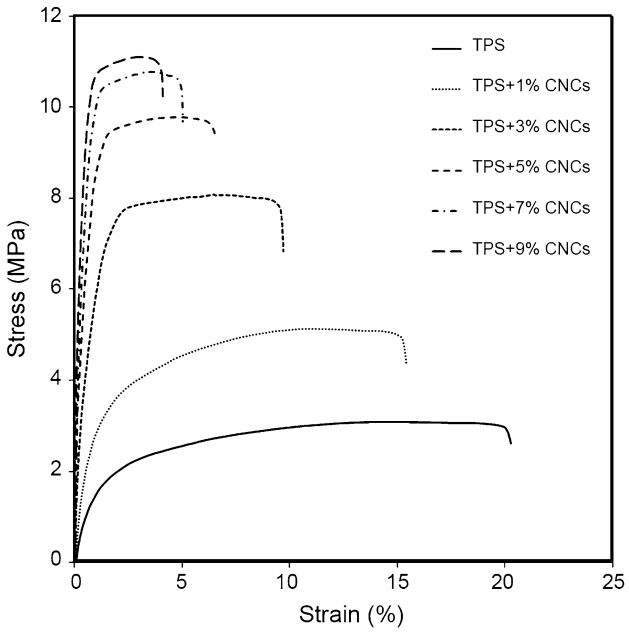

Fig. 8 Stress–strain curves for the neat TPS and its TPS/CNC nanocomposites

added into the TPS matrix after 6 min of mixing to prepare reinforced TPS specimens. The incorporation of CNCs into the starch matrix considerably increased the applied torque, although the torque value decreased again by further mixing. It should be mentioned that the torque value of all the reinforced specimens reached an approximately constant value after 8 min of mixing. In fact, the ultimate torque value is independent of the CNC level. This behavior may be related to the relative appropriate distribution of CNCs in the matrix. However, the incorporation of the CNCs into the TPS matrix enhanced the ultimate torque when compared to the neat TPS without any reinforcement. The occurrence of new filler–polymer interaction in the nanocomposites enhanced the required torque during melt mixing.

Mechanical behavior

Typical stress–strain curves for the neat TPS and its composites with various CNC levels are shown in Fig. 8. Generally, there are two specific regions with two different deformation behavior in the stress–strain curves. At low strains, below 2 %, the stress increased rapidly with the increasing strain and showed a steep slope, which indicated the resistance of chains against the returnable elongation in the elastic region. At higher strains, a slow increase in stress was observed without any necking until the specimen was broken. This behavior can be attributed to a relatively homogeneous structure of the resultant CNC-reinforced TPS specimen [43].

Tensile strength, elongation at break, and Young's modulus of the neat and reinforced TPS specimens are summarized in Table 4. The incorporation of 9 wt% CNC increased the tensile strength at break (σ_b) of the neat TPS from 3.08 to 11.14 MPa. These results were in agreement with the results obtained by Liu et al. [29]. However, the nanocomposites prepared by twin-screw extruder with stronger shear mixing efficiency in comparison with the internal mixer led to improved tensile properties [27]. During the blending process, the amorphous regions of the CNCs swelled by the plasticizer form a strong interaction with the matrix. Such interaction is mostly due to similarity in the polysaccharide structure of the starch and CNCs. As shown in Fig. 9, increasing the CNC content up to 5 wt% considerably enhanced the σ_b value, while beyond this limit the value was slowly increased. This behavior can be related to the agglomeration and poor distribution of the CNCs inside the matrix, which arises from the phase separation in the composite specimens at higher CNC levels. Hence, the performance of CNCs as a reinforcement in the TPS matrix depends on the loading level. As expected, the tensile strength decreased with increasing CNC content.

Figure 9 represents the dependence of the elongation at break (ε_b) versus CNC level. As shown, the introduction of 9 wt% CNC in the TPS lowered the ε_b from 20 % to below 5 %. Amylopectin molecules were stabilized at the starch/cellulose interface, and some interfacial physical joints were established to reduce the mobility of the chains and, consequently, the ε_b value was lowered. In addition,

Table 4 Mechanical properties of the neat TPS and its composites with CNCs (σ_c: tensile strength at break, ε_b: elongation at break, E: Young's modulus)

Code	σ_c (MPa)	ε_b (%)	E (MPa)
TPS	3.08 ± 0.32	20.04 ± 1.98	237.26 ± 19.04
TPS + 1 % CNC	5.14 ± 0.40	15.17 ± 1.21	518.84 ± 31.38
TPS + 3 % CNC	8.06 ± 0.77	9.54 ± 1.10	1293.64 ± 101.28
TPS + 5 % CNC	9.77 ± 0.74	6.53 ± 0.78	2292.52 ± 113.71
TPS + 7 % CNC	10.78 ± 0.82	4.96 ± 0.39	3333.06 ± 240.64
TPS + 9 % CNC	11.14 ± 1.05	4.03 ± 0.41	4231.81 ± 253.82

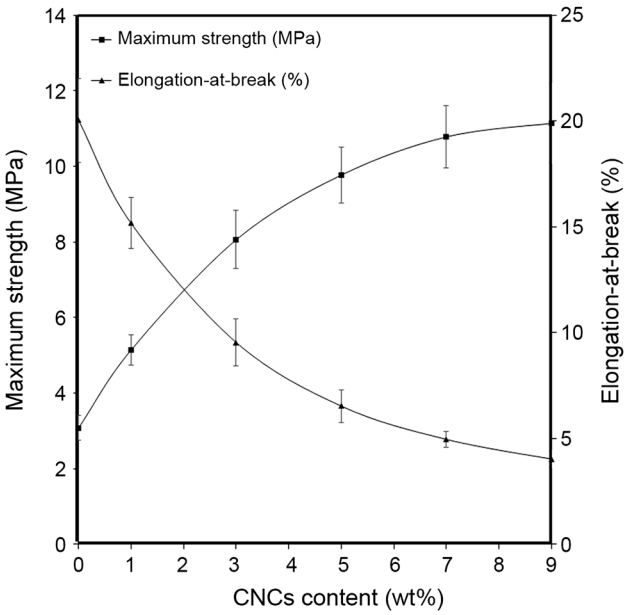

Fig. 9 Tensile strength and elongation at break for the neat TPS and its composites with CNCs

structural defects especially at higher CNC loading level resulted in more heterogeneous structure and stress concentration build-up, which lowered the ε_b value.

Figure 10 shows the variations of Young's modulus (E) versus CNC content. Modulus values had a drastic quasi-linear increase with increasing CNC loading level. Adding 9 wt% CNCs exhibited the highest modulus of elasticity, 17.8 times higher than that of the neat TPS. This increase was due to the nature of the CNCs with high elastic modulus in the polymer matrix.

Effect of CNC content on the T_g and viscoelastic behavior of TPS

DMTA analysis was used to determine the T_g of the neat TPS and its composites with various CNC contents. Figure 11 represents the loss tangential factor (tan δ)

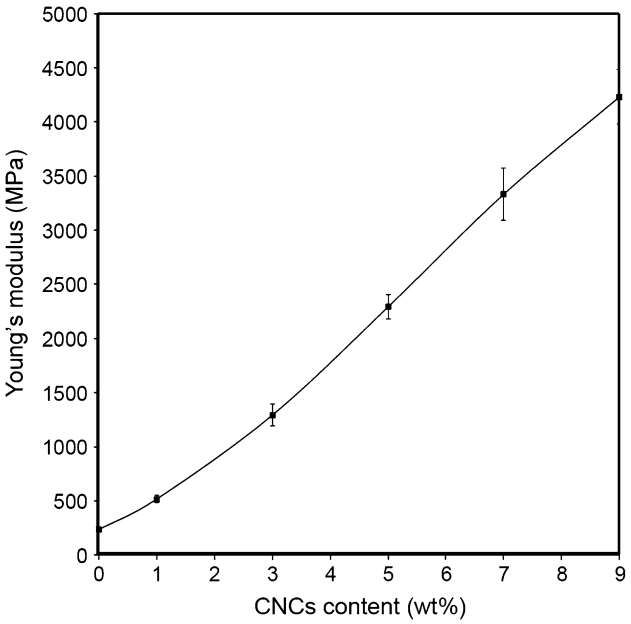

Fig. 10 Variations of Young modulus with increasing CNC content

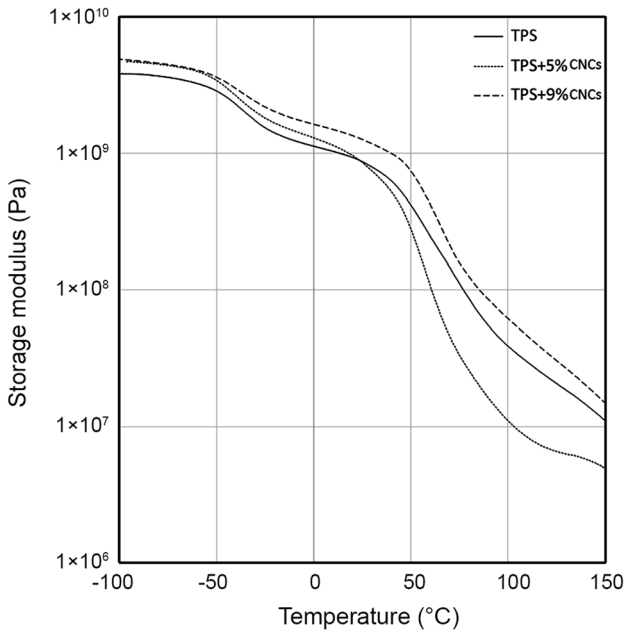

Fig. 11 Effect of CNC level on the storage modulus of the TPS

variation versus temperature for the specimens with 0, 5, and 9 wt% CNCs. Table 5 indicates the T_g of the neat TPS and its composites with different levels of CNCs. As shown, the specimens illustrated two relatively wide peaks on the tan δ curves. It is worth mentioning that the corresponding temperatures of the peaks are usually assumed to be the same as the T_g values of the phases. The high-temperature

Table 5 Glass transition temperatures of the neat TPS and its composites with CNCs

Code	$T_{g,\alpha}$ (°C)	$T_{g,\beta}$ (°C)
TPS	69.2	−40.6
TPS + 5 % CNC	80.8	−40.5
TPS + 9 % CNC	90.7	−40.2

relaxation is attributed to the T_g of TPS-rich domain ($T_{g,\alpha 1}$) and the low-temperature relaxation is related to the T_g of glycerol-rich domain ($T_{g,\alpha 2}$). As shown in Table 5, $T_{g,\alpha 2}$ is highly dependent on the free glycerol concentration in the glycerol-rich domain resulted from the phase separation in the specimens. Averous and Boquillon [44] have reported that the $T_{g,\alpha 2}$ reduced with increasing glycerol content. The glycerol-rich domain which can be widened with increasing glycerol content has more molecular mobility and, consequently, showed less $T_{g,\alpha 2}$ value. It was observed that the $T_{g,\alpha 2}$ was slightly increased with increasing CNC content.

In fact, no significant change in glycerol-rich phase was observed with increasing CNC level. This behavior implied that the CNCs had higher tendency in the TPS-rich phase than in the glycerol-rich phase. In addition, the unchangeable nature of the glycerol molecules which migrated to the interface in the nanocomposites caused a rather constant $T_{g,\alpha 2}$ value to be observed. The same $T_{g,\alpha 2}$ value close to −50 °C was reported in previously published literatures [45, 46]. On the contrary, adding the CNCs at the highest level to the TPS considerably enhanced the $T_{g,\alpha 1}$ from 69.2 to 90.7 °C. A stronger interaction at the starch/cellulose interface reduced the mobility of the starch chains and made the chains more confined. This confinement led to a more rigid system and thus increased the $T_{g,\alpha 1}$ value. In addition, increasing the CNC content broadened the high-temperature peak which indicated a more heterogeneous structure.

Figure 12 represents the temperature dependence of the storage modulus (G′). As can be seen, the higher filler loading exhibited higher storage modulus. This behavior can be attributed to a proper interfacial interaction between TPS and CNCs, which decreases the mobility of the starch chains in the matrix. However, the storage modulus was reduced with increasing temperature, especially for the 5 wt% CNC nanocomposite, due to the chain slippage over the nanocrystals. Increasing the temperature weakened the hydrogen-bonding interaction between the starch and CNCs and caused a probable chain slippage.

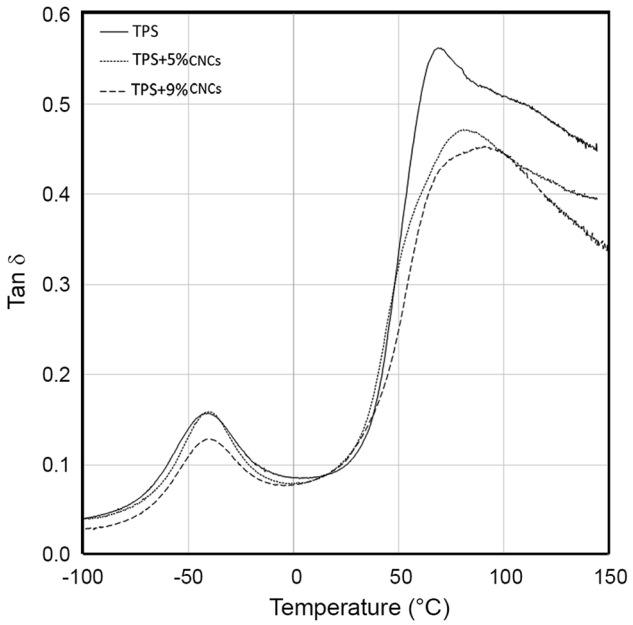

Fig. 12 Effect of CNC level on the loss tangential factor (tan δ) of the neat TPS

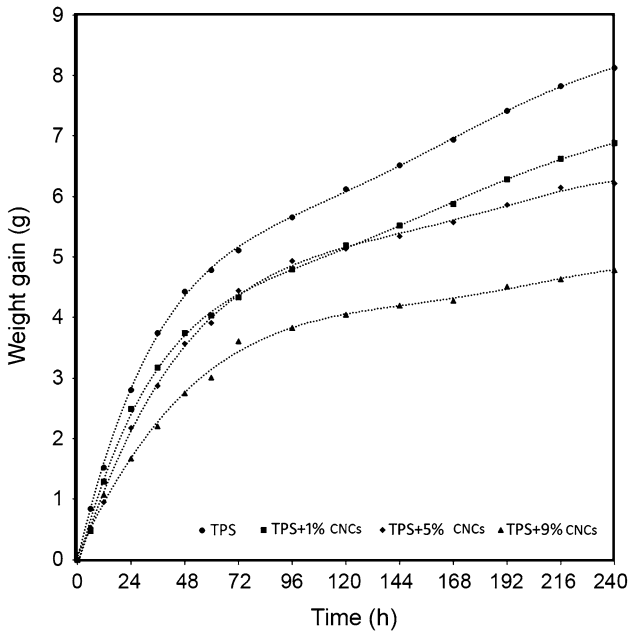

Fig. 13 Weight variation of the TPS and TPS/CNC nanocomposite films versus time held in a humid condition, saturated vapor at 30 °C

Water vapor permeability (WVP)

As it is known, starch is not soluble in water at room temperature, while a TPS sheet is much more soluble and hydrophilic due to the change occurred in the crystalline structure of starch. Figure 13 shows the excess weight of the neat and composite TPS films used in the water vapor permeability test after 10 days. As shown, in the early hours before 72 h the film weights were raised quickly, but beyond this time the weight increases follow a relatively

Table 6 Barrier properties of the neat TPS film and its composites with CNCs

Code	Slope × 10^2 (g h^{-1})	R^2	WVTR (g h^{-1} m^{-2})	WVP × 10^6 (g h^{-1} m^{-1} Pa^{-1})
TPS	1.797	0.9967	14.307	3.372
TPS + 1 % CNC	1.5202	0.9963	12.103	2.853
TPS + 5 % CNC	0.9551	0.9901	7.604	1.792
TPS + 9 % CNC	0.6804	0.9918	5.417	1.277

linear trend. The higher initial slopes in the non-linear portion indicate the higher solubility and diffusion of water molecules into the neat and reinforced TPS films. On the contrary, the previous occupation of a number of active sites through H-bonding between diffused water molecules and the starch chains decreased the slopes in the steady-state (linear) portion of the curves. Besides, the excess weight was non-linearly reduced with increasing CNC content in the nanocomposite films. Slope of the linear part of the weight–time curve, water vapor transmission rate (WVTR), and water vapor permeability (WVP) were calculated and summarized in Table 6.

Adding 9 wt% CNCs to the TPS decreased the WVP from 3.372 × 10^{-6} to 1.277 × 10^{-6} g m^{-1} h^{-1} Pa^{-1} (Fig. 14). In fact, the CNCs could introduce a tortuous path for water vapor molecules to pass through [26, 31]. Additionally, relatively stabilized amylopectin chains at the TPS/CNC interface could improve the WVP decrease in the nanocomposite film [47]. This observation was in contrast to the behavior observed by Dufresne and Vignon [45]. They showed that the reduction of water sorption with cellulose content has a linear trend and cannot be affected by a good interfacial interaction. However, the results obtained by Lu et al. [43] demonstrated a non-linear behavior of water permeation due to low solubility and weak swelling of the cellulose in the water despite its hydrophilic nature. This reality actually refers to the less hydrophilic nature of the CNCs when compared with the starch [27]. Furthermore, adding the cellulose with crystalline nature to the TPS matrix increased the interactions between OH groups of both the polysaccharide structures. These interactions increased the crystalline regions and consequently decreased the hydrophilic nature of the resultant nanocomposite film, especially at higher CNC levels [48–50]. Generally, distributed rigid CNCs in the matrix can act as blocking preventive plates against the water vapor permeation. However, in highly loaded nanocomposite with CNC content higher than 5 wt%, the reduction rate of WVP was considerably decreased. Such behavior may be attributed to the aggregation of CNCs at higher loadings which could lower the barrier efficiency against the water moisture transition through the nanocomposite films.

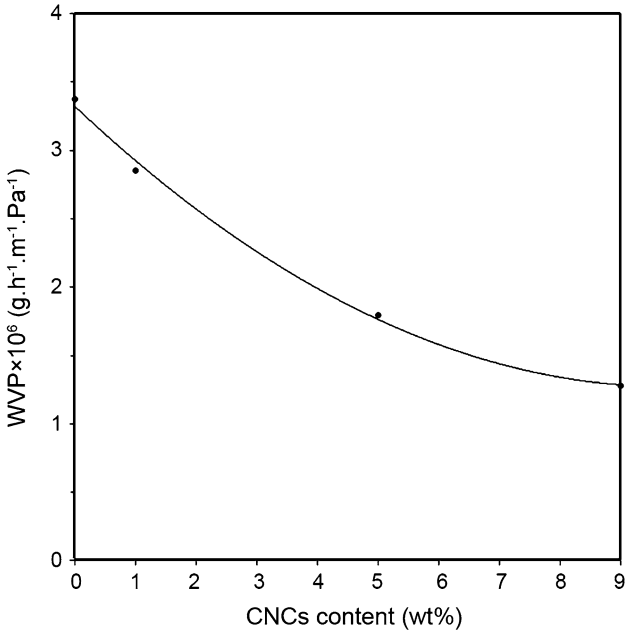

Fig. 14 Water vapor permeability of the neat TPS film and its composite with various CNC levels

Conclusion

Thermoplastic plasticized corn starch (TPS) reinforced at various CNC levels was prepared using an internal mixer. First, the CNCs with proper morphological characteristics were successfully extracted from the MCC via acid hydrolysis process. The microscopy results showed that the hydrolysis of the MCC at 44 °C resulted in CNCs with rod-like morphology and the highest yield and aspect ratio. The CNCs prepared at above hydrolysis temperature were used to prepare reinforced TPS composites with various CNC levels. The mechanical results indicated that increasing the CNC content up to 5 wt% considerably enhanced the σ_b value, while beyond this limit the value was slowly increased. In general, the incorporation of 9 wt% CNCs into the TPS remarkably enhanced the tensile strength from 3.1 to 11.1 MPa (358 % increase) and Young's modulus from 237.3 MPa to 4.2 GPa. In addition, a proper interaction between the CNCs and the matrix considerably shifted the $T_{g,\alpha 1}$ value from 69.2 to 90.7 °C. The moisture

sensitivity was reduced with increasing CNC content in the TPS matrix. The barrier property of the rigid CNC planes lowered the moisture transmission through the resultant nanocomposite films.

Acknowledgments The partial financial support from the Iranian Nanotechnology Initiative and the Vice President for Research and Technology of Iran University of Science and Technology (IUST) is gratefully appreciated.

References

1. Lu DR, Xiao CM, Xu SJ (2009) Starch-based completely biodegradable polymer materials. Express Polym Lett 3:366–375
2. Jiménez A, Fabra MJ, Talens P, Chiralt A (2012) Edible and biodegradable starch films: a review. Food Bioprocess Tech 5:2058–2076
3. Teixeira EdM, Curvelo AAS, Corrêa AC, Marconcini JM, Glenn GM, Mattoso LHC (2012) Properties of thermoplastic starch from cassava bagasse and cassava starch and their blends with poly (lactic acid). Ind Crop Prod 37:61–68
4. Bagdi K, Müller P, Pukánszky B (2006) Thermoplastic starch/layered silicate composites: structure, interaction, properties. Compos Interfaces 13:1–17
5. Sinharay S, Bousmina M (2005) Biodegradable polymers and their layered silicate nanocomposites: in greening the 21st century materials world. Prog Mater Sci 50:962–1079
6. Taghizadeh A, Favis BD (2013) Carbon nanotubes in blends of polycaprolactone/thermoplastic starch. Carbohydr Polym 98:189–198
7. Castrejón-Parga KY, Camacho-Montes H, Rodríguez-González CA, Velasco-Santos C, Martínez-Hernández AL, Bueno-Jaquez D, Rivera-Armenta JL, Ambrosio CR, Conzalez CC, Mendoza-Duarte ME, García-Casillas PE (2014) Chitosan–starch film reinforced with magnetite-decorated carbon nanotubes. J Alloy Compd 615:S505–S510
8. Cheng J, Zheng P, Zhao F, Ma X (2013) The composites based on plasticized starch and carbon nanotubes. Int J Biol Macromol 59:13–19
9. Nafchi AM, Alias AK, Mahmud S, Robal M (2012) Antimicrobial, rheological, and physicochemical properties of sago starch films filled with nanorod-rich zinc oxide. J Food Eng 113:511–519
10. Pradhan GC, Dash S, Swain SK (2014) Effect of zirconium oxide nanopowder on the thermal, chemical and gas barrier properties of starch. Mater Sci Semicond Process 23:115–121
11. Ma X, Chang PR, Yu J, Lu P (2008) Characterizations of glycerol plasticized-starch (GPS)/carbon black (CB) membranes prepared by melt extrusion and microwave radiation. Carbohydr Polym 74:895–900
12. Ma T, Chang PR, Zheng P, Ma X (2013) The composites based on plasticized starch and graphene oxide/reduced graphene oxide. Carbohydr Polym 94:63–70
13. Peregrino PP, Sales MJ, da Silva MF, Soler MA, da Silva LF, Moreira SG, Paterno LG (2014) Thermal and electrical properties of starch-graphene oxide nanocomposites improved by photochemical treatment. Carbohydr Polym 106:305–311
14. Pérez CJ, Alvarez VA, Mondragón I, Vázquez A (2007) Mechanical properties of layered silicate/starch polycaprolactone blend nanocomposites. Polym Int 56:686–693
15. Pérez CJ, Alvarez VA, Mondragón I, Vázquez A (2008) Water uptake behavior of layered silicate/starch–polycaprolactone blend nanocomposites. Polym Int 57(2):247–253
16. Pérez CJ, Alvarez VA, Vázquez A (2008) Creep behaviour of layered silicate/starch–polycaprolactone blends nanocomposites. Mater Sci Eng A 480:259–265
17. Mortazavi S, Ghasemi I, Oromiehie A (2013) Prediction of tensile modulus of nanocomposites based on polymeric blends. Iran Polym J 22:437–445
18. Liu Z, Zhao L, Chen M, Yu J (2011) Effect of carboxylate multiwalled carbon nanotubes on the performance of thermoplastic starch nanocomposites. Carbohydr Polym 83:447–451
19. Li R, Liu C, Ma J (2011) Studies on the properties of graphene oxide-reinforced starch biocomposites. Carbohydr Polym 84:631–637
20. Moon RJ, Martini A, Nairn J, Simonsen J, Youngblood J (2011) Cellulose nanomaterials review: structure, properties and nanocomposites. Chem Soc Rev 40:3941–3994
21. Camacho F, González-Tello P, Jurado E, Robles A (1996) Microcrystalline-cellulose hydrolysis with concentrated sulphuric acid. J Chem Technol Biotechnol 67:350–356
22. Das K, Ray D, Bandyopadhyay NR, Ghosh T, Mohanty AK, Misra M (2009) A study of the mechanical, thermal and morphological properties of microcrystalline cellulose particles prepared from cotton slivers using different acid concentrations. Cellulose 16:783–793
23. Dong X, Revol J-F, Gray D (1998) Effect of microcrystallite preparation conditions on the formation of colloid crystals of cellulose. Cellulose 5:19–32
24. Krishnamachari P, Hashaikeh R, Chiesa M, Gad El Rab KRM (2012) Effects of acid hydrolysis time on cellulose nanocrystals properties: nanoindentation and thermogravimetric studies. Cellul Chem Technol 46:13–18
25. Bondeson D, Mathew A, Oksman K (2006) Optimization of the isolation of nanocrystals from microcrystalline cellulose by acid hydrolysis. Cellulose 13:171–180
26. Savadekar NR, Mhaske ST (2012) Synthesis of nano cellulose fibers and effect on thermoplastics starch based films. Carbohydr Polym 89:146–151
27. Hietala M, Mathew AP, Oksman K (2013) Bionanocomposites of thermoplastic starch and cellulose nanofibers manufactured using twin-screw extrusion. Eur Polym J 49:950–956
28. Teixeira EdM, Pasquini D, Curvelo AAS, Corradini E, Belgacem MN, Dufresne A (2009) Cassava bagasse cellulose nanofibrils reinforced thermoplastic cassava starch. Carbohydr Polym 78:422–431
29. Liu D, Zhong T, Chang PR, Li K, Wu Q (2010) Starch composites reinforced by bamboo cellulosic crystals. Bioresour Technol 101:2529–2536
30. Nasseri R, Mohammadi N (2014) Starch-based nanocomposites: a comparative performance study of cellulose whiskers and starch nanoparticles. Carbohydr Polym 106:432–439
31. Chang PR, Jian R, Zheng P, Yu J, Ma X (2010) Preparation and properties of glycerol plasticized-starch (GPS)/cellulose nanoparticle (CN) composites. Carbohydr Polym 79:301–305
32. Kaushik A, Singh M, Verma G (2010) Green nanocomposites based on thermoplastic starch and steam exploded cellulose nanofibrils from wheat straw. Carbohydr Polym 82:337–345
33. Aila-Suárez S, Palma-Rodríguez HM, Rodríguez-Hernández AI, Hernández-Uribe JP, Bello-Pérez LA, Vargas-Torres A (2013) Characterization of films made with chayote tuber and potato starches blending with cellulose nanoparticles. Carbohydr Polym 98:102–107
34. González K, Retegi A, González A, Eceiza A, Gabilondo N (2014) Starch and cellulose nanocrystals together into thermoplastic starch bionanocomposites. Carbohydr Polym 117:83–90
35. Prakobna K, Galland S, Berglund LS (2014) High-performance and moisture-stable cellulose-starch nanocomposites based on bioinspired core–shell nanofibers. Biomacromolecules 16:904–912

36. Cao X, Chen Y, Chang P, Muir A, Falk G (2008) Starch-based nanocomposites reinforced with flax cellulose nanocrystals. Express Polym Lett 2:502–510
37. Leung ACW, Lam E, Chong J, Hrapovic S, Luong JHT (2013) Reinforced plastics and aerogels by nanocrystalline cellulose. J Nanopart Res 15:1636. doi:10.1007/s11051-013-1636-z
38. Voskoboinikov IV, Konstantinova SA, Korotkov AN, Gal'braikh LS (2011) Process for preparing nanocrystalline cellulose. Fiber Chem 43:125–128
39. Kontturi E, Johansson L-S, Kontturi KS, Ahonen P, Thüne PC, Laine J (2007) Cellulose nanocrystal submonolayers by spin coating. Langmuir 23:9674–9680
40. Segal L, Creely JJ, Martin AE, Conrad CM (1959) An empirical method for estimating the degree of crystallinity of native cellulose using the X-Ray diffractometer. Text Res J 29:786–794
41. Kroon-Batenburg LMJ, Kroon J (1997) The crystal and molecular structures of cellulose I and II. Glycoconj J 14:677–690
42. Abbott A, Bismarck A (2010) Self-reinforced cellulose nanocomposites. Cellulose 17:779–791
43. Lu Y, Weng L, Cao X (2006) Morphological, thermal and mechanical properties of ramie crystallites-reinforced plasticized starch biocomposites. Carbohydr Polym 63:198–204
44. Averous L, Boquillon N (2004) Biocomposites based on plasticized starch: thermal and mechanical behaviours. Carbohydr Polym 56:111–122
45. Dufresne A, Vignon MR (1998) improvement of starch film performances using cellulose microfibrils. Macromolecules 31:2693–2696
46. Avérous L, Fringant C, Moro L (2001) Plasticized starch-cellulose interactions in polysaccharide composites. Polymer 42:6565–6572
47. Svagan AJ, Hedenqvist MS, Berglund L (2009) Reduced water vapour sorption in cellulose nanocomposites with starch matrix. Compos Sci Technol 69:500–506
48. Curvelo AAS, de Carvalho AJF, Agnelli JAM (2001) Thermoplastic starch–cellulosic fibers composites: preliminary results. Carbohydr Polym 45:183–188
49. Anglès MN, Dufresne A (2000) Plasticized starch/tunicin whiskers nanocomposites. 1. Structural analysis. Macromolecules 33:8344–8353
50. Anglès MN, Dufresne A (2001) Plasticized starch/tunicin whiskers nanocomposite materials. 2. Mechanical behavior. Macromolecules 34:2921–2931